

Electronic Supplementary Information (ESI)

Unique Vapochromism of a Paddlewheel-type Dirhodium Complex
Accompanied by Dynamic Structural and Phase Transitions

Yusuke Kataoka,^{*,a} Yoshihiro Kohara,^a Natsumi Yano,^b Tatsuya Kawamoto^c

- a) Department of Chemistry, Graduate School of Natural Science and Technology, Shimane University, 1060, Nishikawatsu, Matsue, Shimane, 690-8504.
E-mail: kataoka@riko.shimane-u.ac.jp (Y. Kataoka)
- b) Special Course of Science and Engineering, Graduate School of Natural Science and Technology, Shimane University, 1060, Nishikawatsu, Matsue, Shimane, 690-8504.
- c) Department of Chemistry, Faculty of Science, Kanagawa University, 2946, Tsuchiya, Hiratsuka, Kanagawa, 259-1293, Japan.

Materials and Instruments

All chemicals used in this study were purchased from commercial suppliers and used as received without further purification. $[\text{Rh}_2(\text{O}_2\text{CCH}_3)_4(\text{H}_2\text{O})_2]$ was synthesized according to previously reported method.^{S1}

^1H NMR spectrum was acquired using a JEOL ECS-500SS spectrometer in chloroform-*d* (residual proton signal of chloroform at 7.26 ppm was used as an internal reference). Electrospray ionization (ESI) mass spectroscopy was measured with a Bruker micrOTOF II spectrometer. Infrared (IR) spectra were recorded using a JASCO FT/IR 6300 spectrometer equipped with a JASCO ATR PRO ONE module. Elemental analysis was conducted on a Yanaco CHN CORDER MT-6 installed at Shimane University, Japan. Powder X-ray diffraction (PXRD) analysis was performed on a Rigaku SmartLab X-ray diffractometer with Cu $K\alpha$ radiation. Thermo-gravimetric (TG) analysis was performed under nitrogen atmosphere with a heating rate of 4K/min on a RIGAKU Thermo plus EVO2 system. Differential scanning calorimetry (DSC) measurements was conducted on a RIGAKU Thermo plus EVO2 DSC 8231 system in the temperature range from 300 to 423 K with a heating rate of 10K/min under nitrogen atmosphere. Diffuse reflectance (DR) spectrum was measured with a JASCO V-670 spectrometer equipped with a JASCO ISN-923 integrating sphere.

Synthesis of $[\text{Rh}_2(\text{HA})_4]_n$ (1G)

A mixture of $[\text{Rh}_2(\text{O}_2\text{CCH}_3)_4(\text{H}_2\text{O})_2]$ (191.2 mg, 0.400 mmol), hexanoic acid (2.0 mL, 16.0 mmol), and chlorobenzene (15.0 mL) was heated at 413 K for 24 h under nitrogen atmosphere. The reactant was transferred into 200 cm³ separating funnel and washed with 0.10 M Na_2CO_3 aqueous solution to remove the unreacted hexanoic acid. Then, the resulting solution (oil phase) was evaporated to dryness, and obtained residue was further purified by a silica-gel column chromatography (eluent: 3% MeOH in CHCl_3). After the evaporation of the solvent, the green residue was recrystallized from THF, and obtained green microcrystals were dried at 373 K for 3 h. Yield: 261.7 mg (0.393 mmol, 98.2%). Anal. Calc. for $\text{Rh}_2\text{C}_{24}\text{H}_{44}\text{O}_8$: C, 43.26%; H, 6.65%. Found: C, 43.43%; H, 6.90%. ^1H NMR (500 MHz, 300 K, CDCl_3) δ = 2.32 (t, 8H), 1.55 (q, 8H), 1.20 (m, 16H), 0.82 (t, 12H) ppm. ESI-MS: Calcd for $[\text{M} + \text{Na}]^+$ 689.1038 m/z ; Found 689.1040 m/z . Infrared (ATR, cm^{-1}): 2952 (m), 2929 (m), 2871 (m), 1565 (vs), 1522 (m), 1410 (vs), 1374 (w), 1343 (m), 1309 (m), 1229 (w), 1211 (vw), 1192 (w), 1110 (w), 1055 (vw), 1006 (vw), 956 (vw), 917 (vw), 891 (vw), 844 (vw), 803 (vw), 738 (s), 678 (s), 639 (vw), 594 (vw).

Synthesis of $[\text{Rh}_2(\text{HA})_4(\text{py})_2]$ (**1R**)

Method A (vapochromic experiment).

1G (199.2 mg, 0.300 mmol) was immediately changed to red powder through uneven purple powder by the exposure of pyridine vapor at room temperature in closed glass vessel. Obtained red powder was dried under vacuum at 300 K for 2 h. Yield: 246.3 mg (0.299 mmol, 99.6 %).

Method B (synthesis in solution).

The green color of CHCl_3 solution containing **1G** (199.2 mg, 0.30 mmol) was immediately changed to red color by the addition of pyridine (0.50 mL, 4.00 mmol). After 1 h stirring, obtained red solution was evaporated to dryness, and red residue was dried under vacuum at 300 K for 2 h. Yield: 241.8 mg (0.293 mmol, 97.7%).

Characterization of **1R**.

Anal. Calc. for $\text{Rh}_2\text{C}_{34}\text{H}_{54}\text{N}_2\text{O}_8$: C, 49.52; H, 6.60; N, 3.40%. Found: C, 49.70; H, 6.87; N, 3.41%. ^1H NMR (500 MHz, 300 K, CDCl_3) δ = 9.29 (d, 4H), 7.99 (tt, 2H), 7.66 (m, 4H), 2.12 (t, 8H), 1.45 (q, 8H), 1.22 (m, 8H), 1.12 (m, 8H), 0.83 (t, 12H) ppm. Infrared (ATR, cm^{-1}): 3068 (vw), 2925 (m), 2863 (m), 1585 (vs), 1446 (m), 1412 (vs), 1341 (m), 1315 (m), 1215 (m), 1149 (vw), 1108 (vw), 1065 (w), 1032 (w), 1006 (w), 953 (vw), 889 (vw), 847 (vw), 803 (vw), 725 (s), 696 (vs), 675 (s), 620 (s).

Synthesis of $[\text{Rh}_2(\text{HA})_4(\text{py})_2]$ (**1P**)

Purple powder of **1P** was obtained by the heating of **1R** (41.2 mg, 0.0500 mmol) under vacuum at 338 K for 1 h. Yield: 37.0 mg (0.0497 mmol, 99.2%). Anal. Calc. for $\text{Rh}_4\text{C}_{58}\text{H}_{98}\text{N}_2\text{O}_{16}$: C, 46.72; H, 6.62; N, 1.88%. Found: C, 46.83; H, 6.45; N, 1.96%. ^1H NMR (500 MHz, 300 K, CDCl_3) δ = 9.20 (d, 4H), 8.05 (tt, 2H), 7.70 (m, 4H), 2.14 (t, 16H), 1.45 (q, 16H), 1.22 (m, 16H), 1.11 (m, 16H), 0.83 (t, 24H) ppm. Infrared (ATR, cm^{-1}): 2954 (m), 2926 (m), 2868 (m), 1577 (vs), 1523 (vw), 1485 (w), 1448 (m), 1410 (vs), 1314 (w), 1374 (w), 1221 (w), 1190 (vw), 1154 (vw), 1110 (w), 1077 (w), 1037 (w), 1011 (vw), 983 (vw), 891 (vw), 849 (vw), 761 (m), 698 (s), 676 (m), 632 (w), 590 (w).

Single crystal X-ray diffraction analyses

Single crystals of **1G** and **1R** suitable for single crystal X-ray diffraction analyses were obtained by the slow evaporation from THF solution of **1G** and pyridine solution of **1R**, while those of **1P** were obtained by slow diffusion of water into ethanol solution of **1P**. Diffraction data of **1G** and **1P** were collected at 150 K on a RIGAKU Saturn 724 CCD system equipped with Mo rotating-anode X-ray generator with monochromated Mo- $K\alpha$ radiation ($\lambda = 0.71075 \text{ \AA}$) installed in Kanagawa University and were processed with CrysAlisPro program, while those of **1R** were collected at 150 K on a RIGAKU XtaLAB AFC11 system equipped with Mo rotating-anode X-ray generator with monochromated Mo- $K\alpha$ radiation installed in Institute of Molecular Science and were processed with CrysAlisPro program. The structures of **1G**, **1R**, and **1P** were solved by SIR-2004,^{S2} SIR-2011,^{S3} and SHELXT^{S4} methods, respectively, and refined using the full-matrix least-squares technique F^2 with SHELXL2014^{S5} equipped in the RIGAKU CrystalStructure software. Non-hydrogen atoms were refined with anisotropic displacement and almost all of hydrogen atoms were located at the calculated positions and refined as riding models. Crystal data as well as the details of data collection and refinement for **1G**, **1R**, and **1P** can be obtained as CIFs from Cambridge Crystallographic Data Center (CCDC). Deposition numbers of **1G**, **1R**, and **1P** are CCDC-2018470, 2018471, and 2018472, respectively.

Theoretical calculations

All density functional theory (DFT) calculations were performed by using the restricted B3LYP functional combined with SDD basis for Rh ions and cc-pVDZ for other atoms on the Gaussian 09 program.^{S6} The molecular geometries of Rh₂ complexes of **1R** and **1P** were initially obtained from their CIFs, and then their geometries were fully optimized and checked by vibrational frequency analyses. On the other hand, we designed the [Rh₂(HA)₄(H₂O)₂], in which two H₂O ligands are coordinated to the axial sites of Rh₂ bond, as the model structure of **1G** by using the CIF of **1G**, and then its geometry was fully optimized and checked by vibrational frequency analysis. Vertical singlet excitations were calculated by means of time-dependent DFT (TDDFT) method.

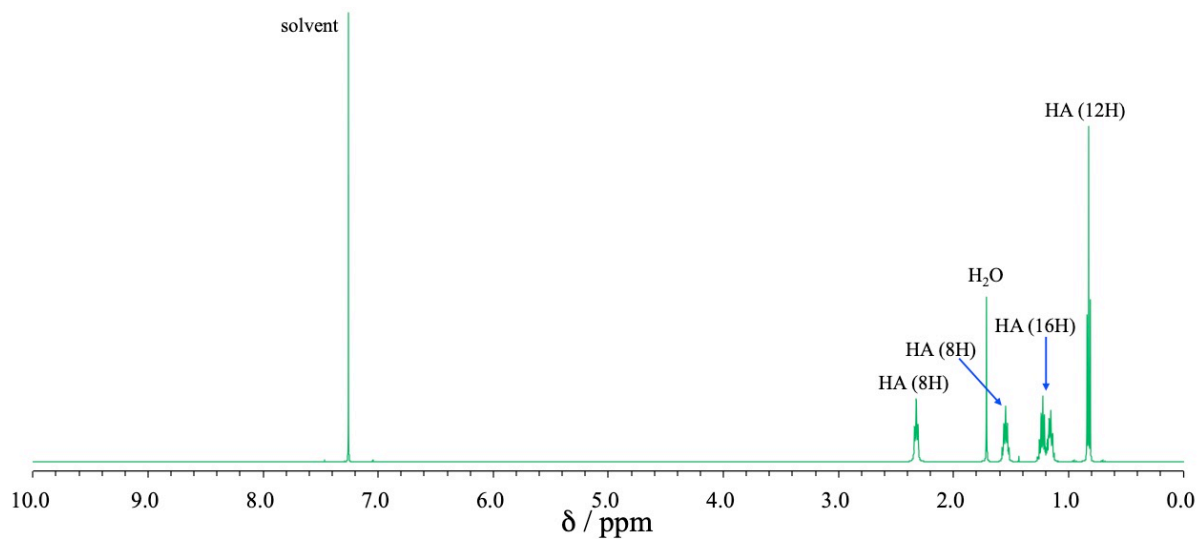


Fig. S1 ¹H NMR spectrum of **1G** in CDCl₃.

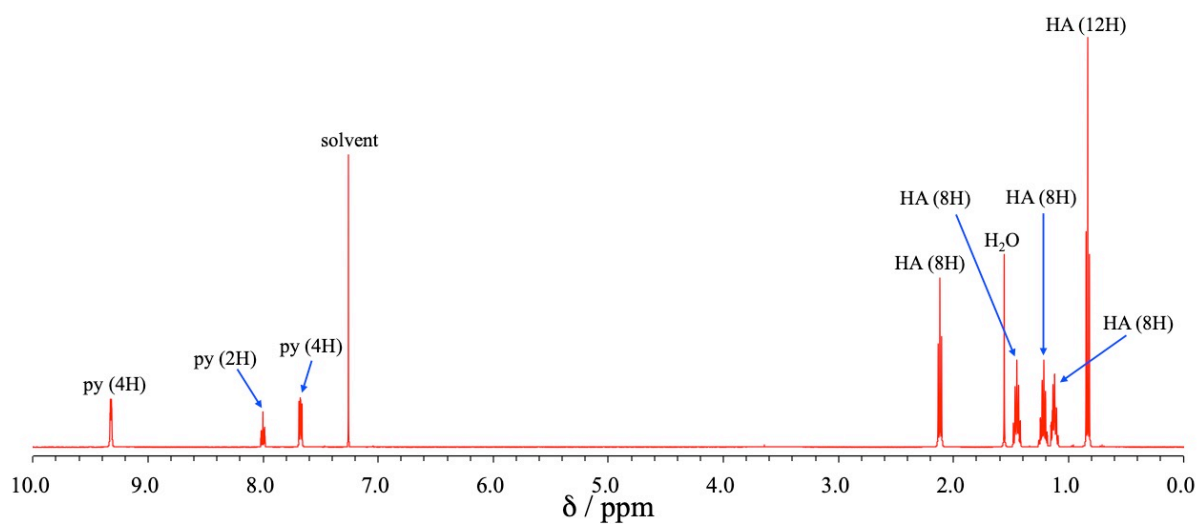


Fig. S2 ¹H NMR spectrum of **1R** in CDCl₃.

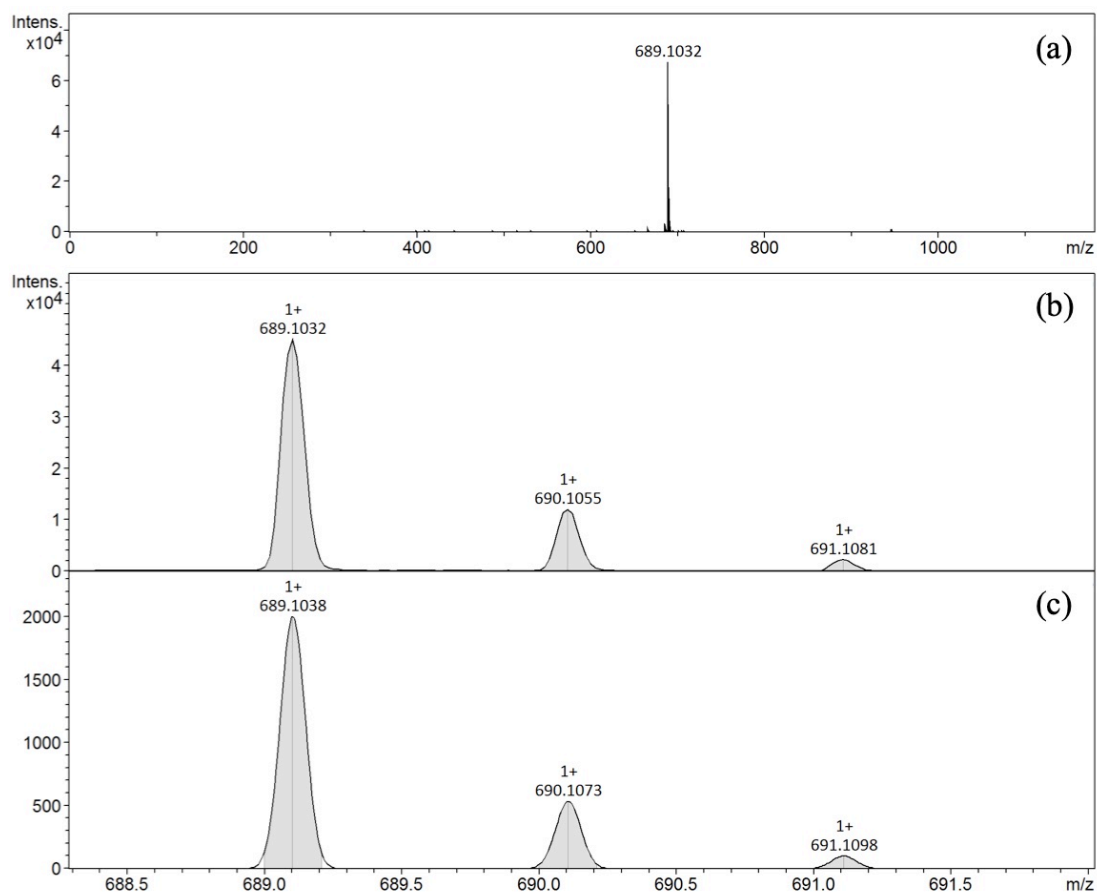


Fig. S3 ESI-MS (positive ion mode) of **1G**; (a) observed wide-scan spectrum, (b) observed peaks, and (c) simulated peaks.

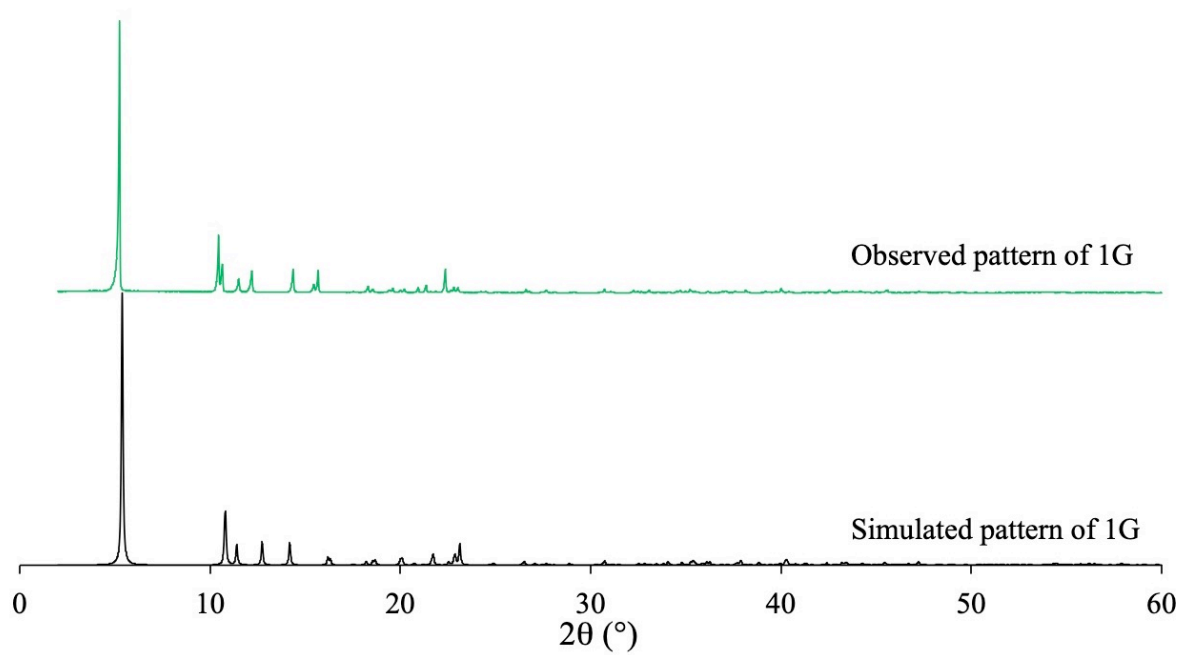


Fig. S4 Observed and simulated XRD patterns of **1G**.

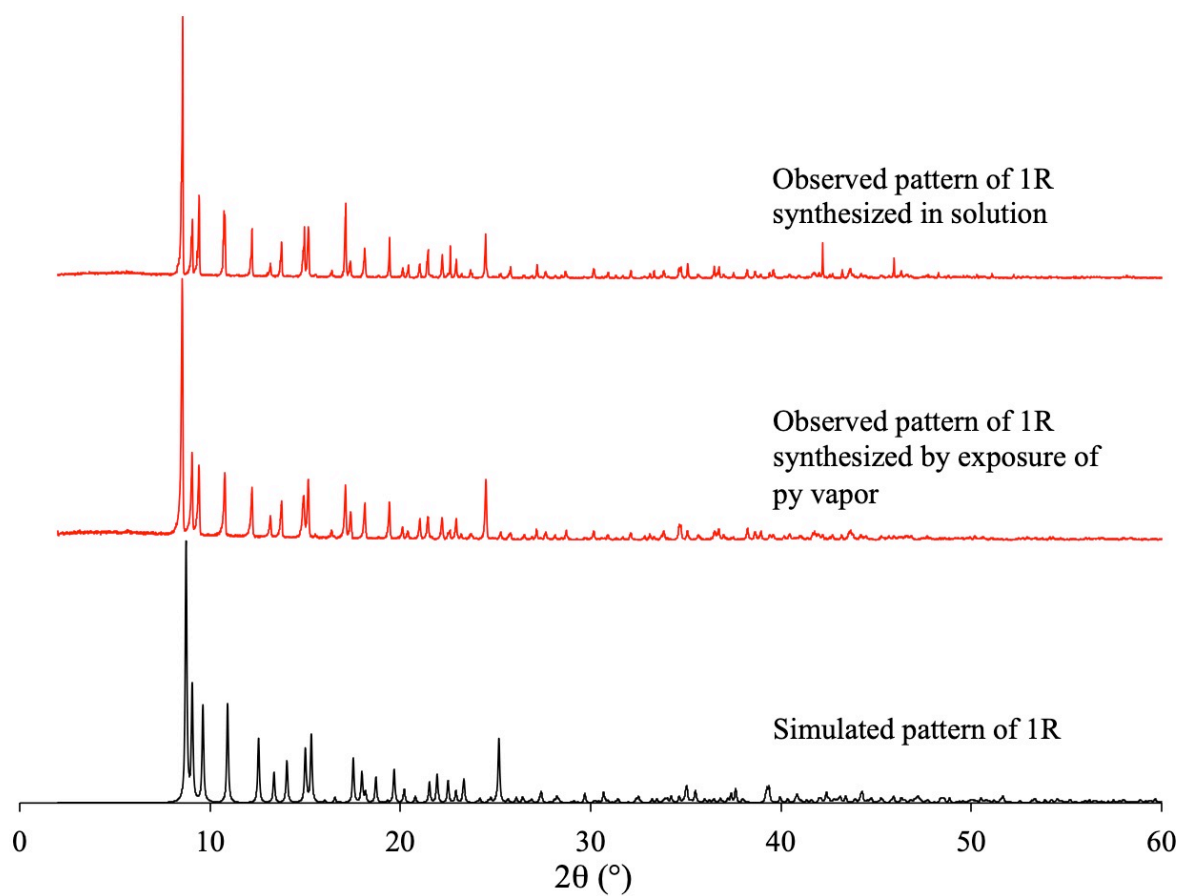


Fig. S5 Observed and simulated XRD patterns of **1R**.

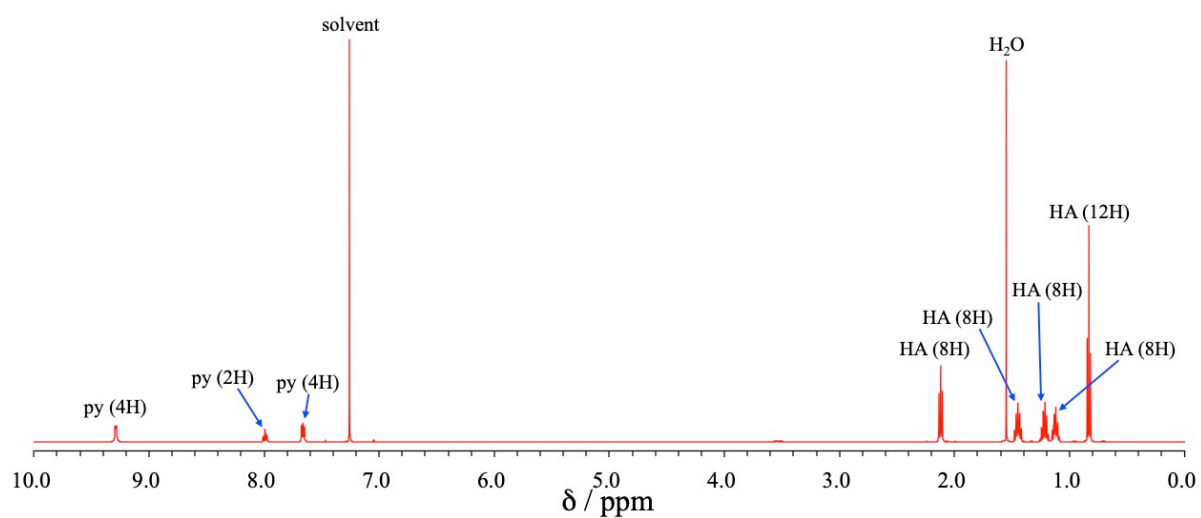


Fig. S6 ^1H -NMR spectrum of **1R**, which is prepared by exposure of py vapor to **1G**, in CDCl_3 .

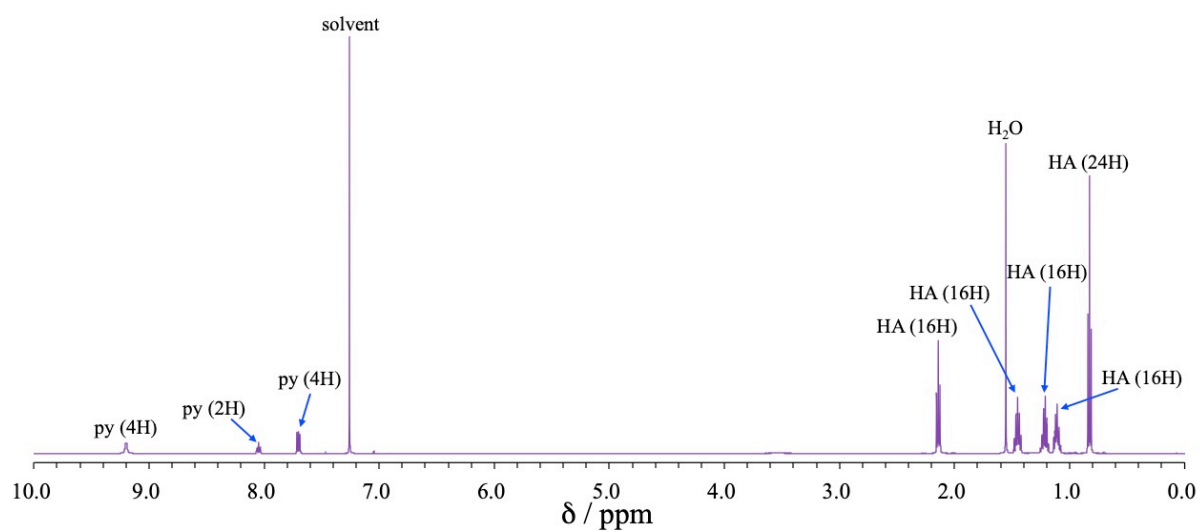


Fig. S7 ^1H NMR spectrum of **1P** in CDCl_3 .

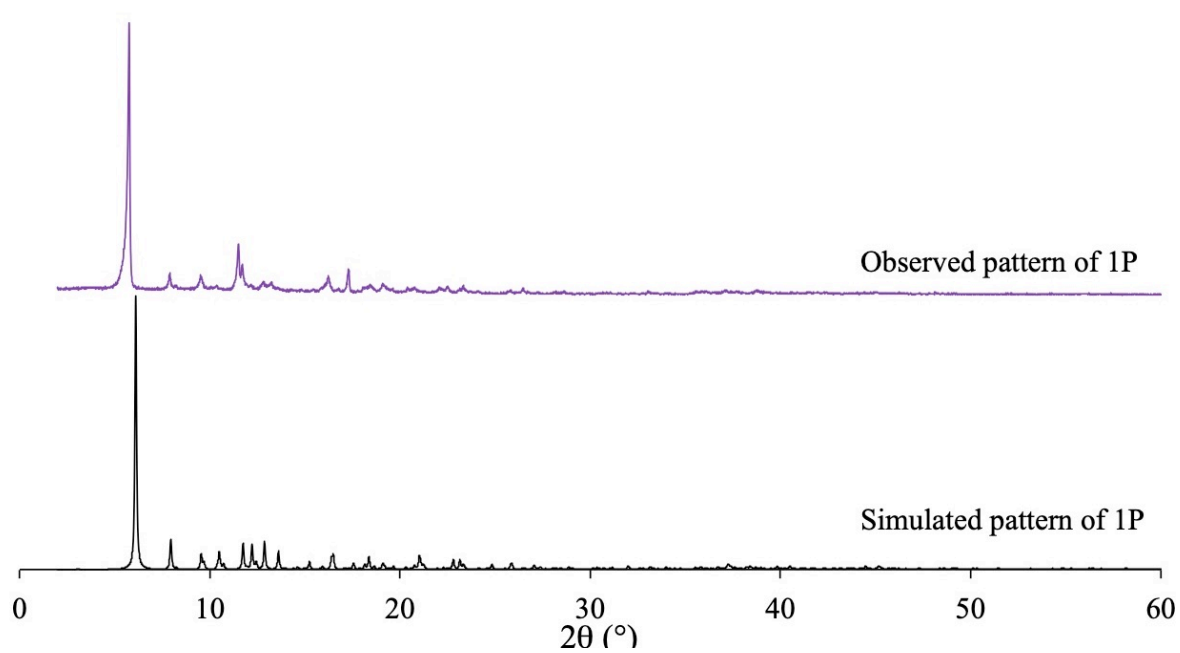


Fig. S8 Observed and simulated XRD patterns of **1P**.

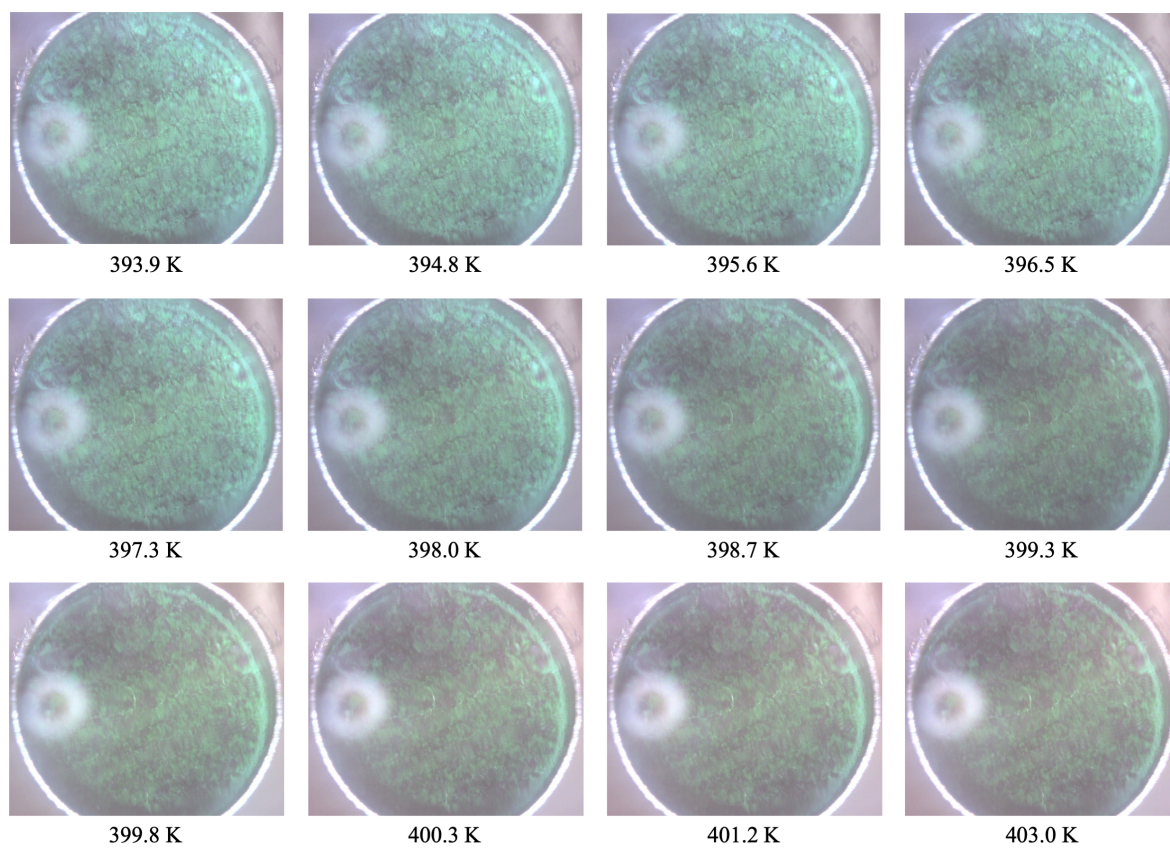


Fig. S9 Thermal changes of **1G** in the heating process.

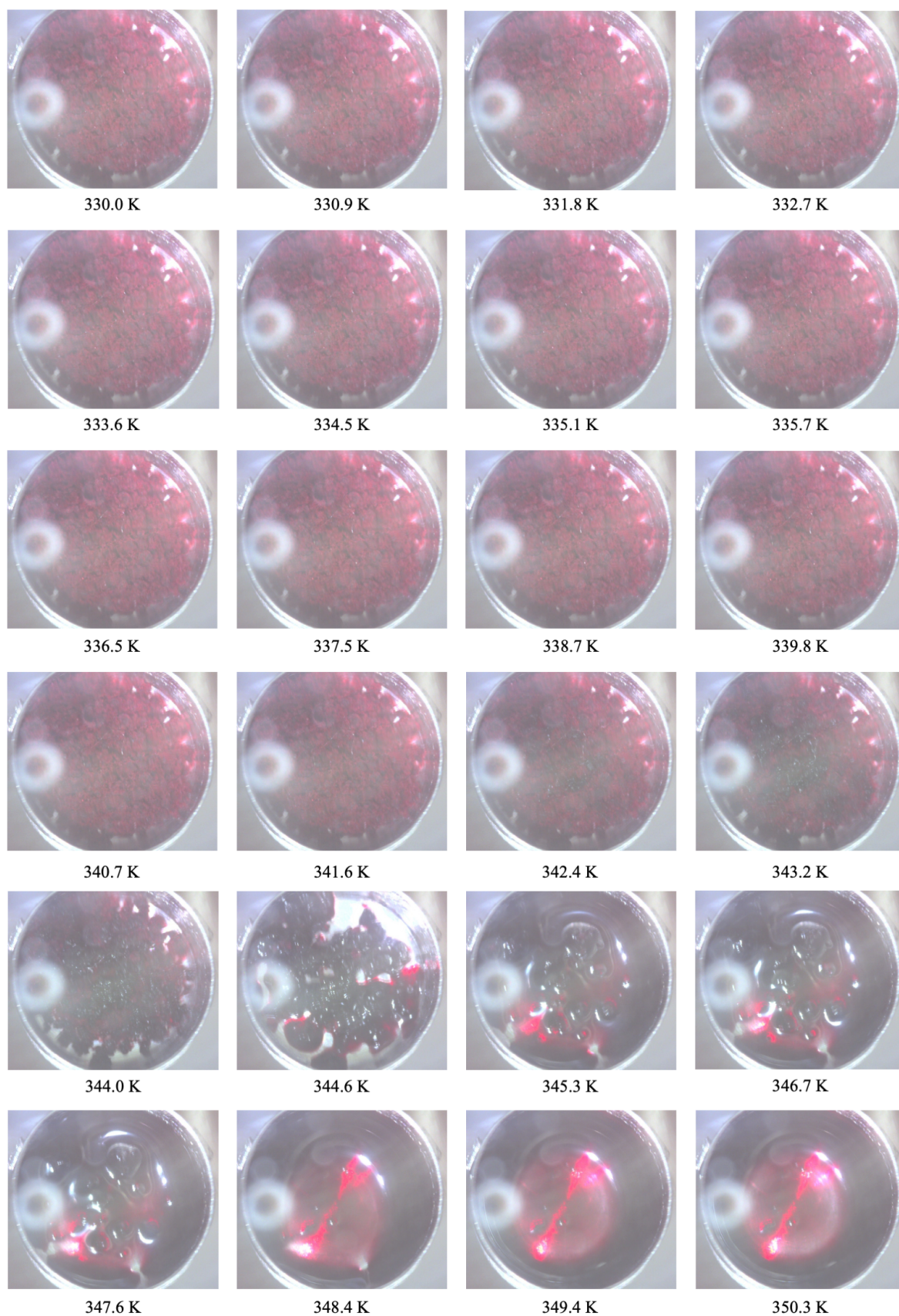


Fig. S10 Thermal changes of **1R** in the heating process.

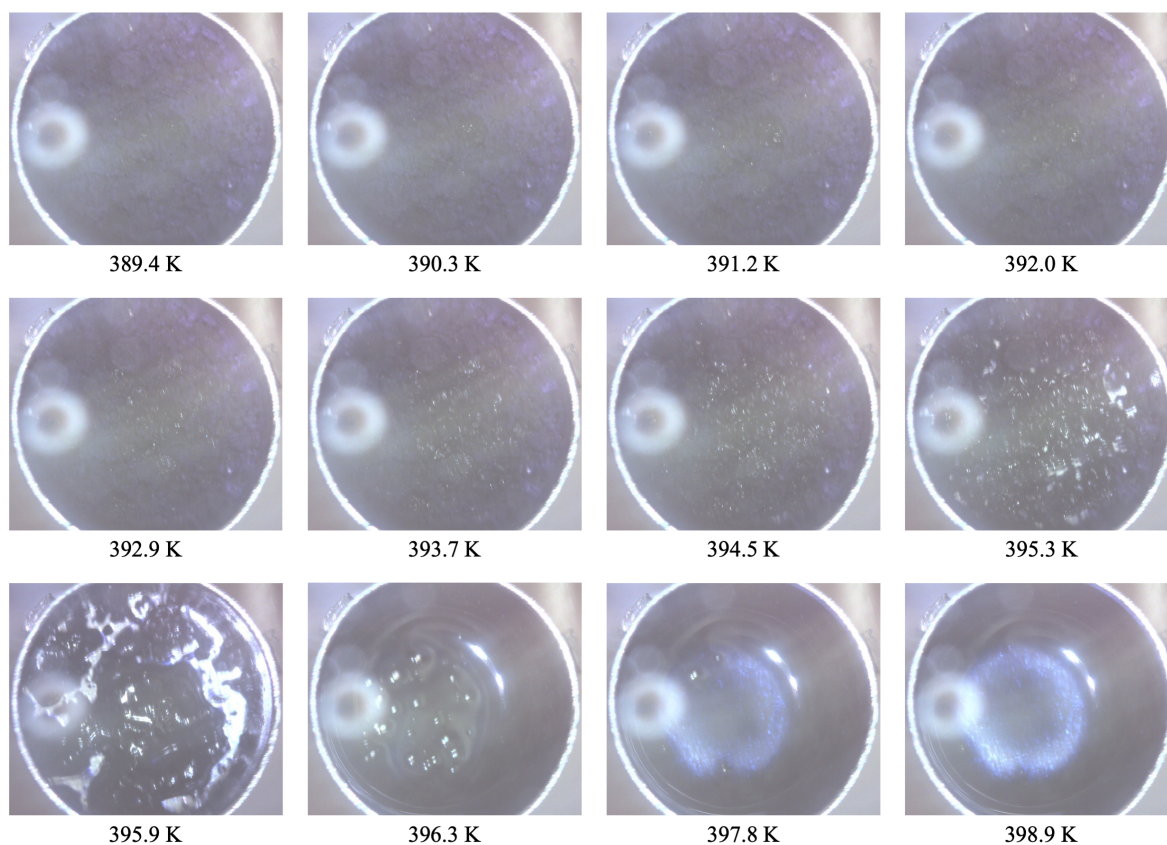


Fig. S11 Thermal changes of **1P** in the heating process.

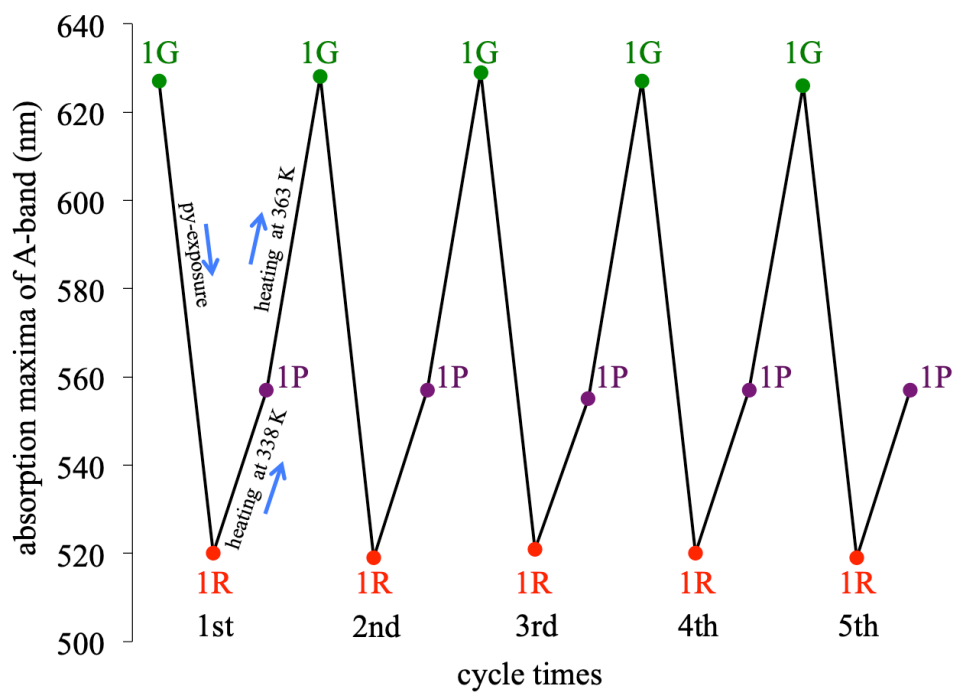


Fig. S12 Reversible pyridine-exposure and heating cycles based on absorption maxima of A-band of **1G**, **1R**, and **1P** in the solid state measured by DR spectra.

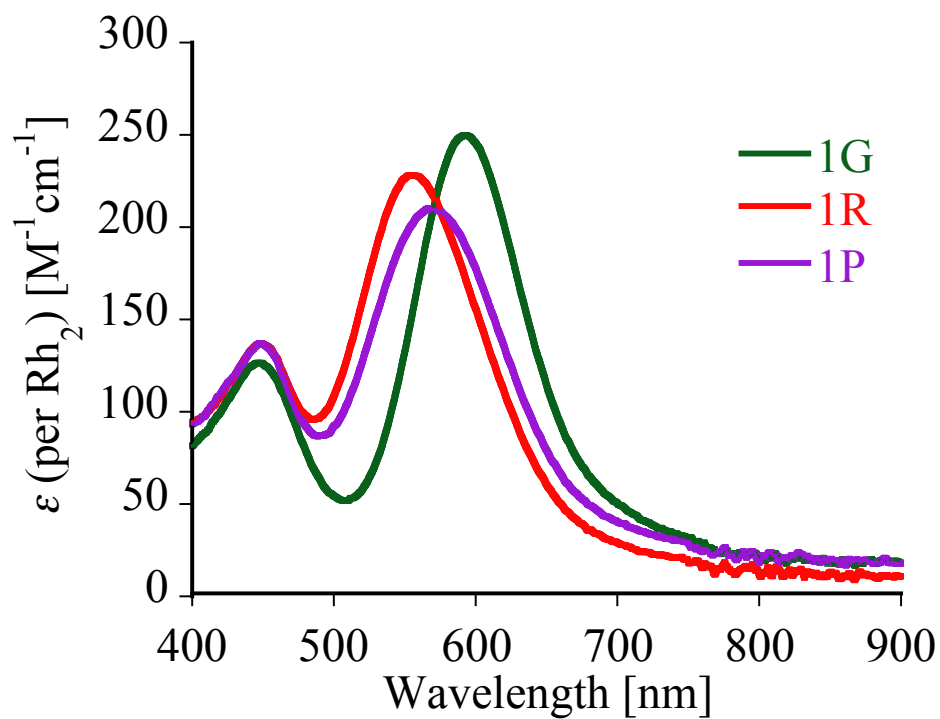


Fig. S13 Absorption spectra of **1G**, **1R**, and **1P** in ethanol.

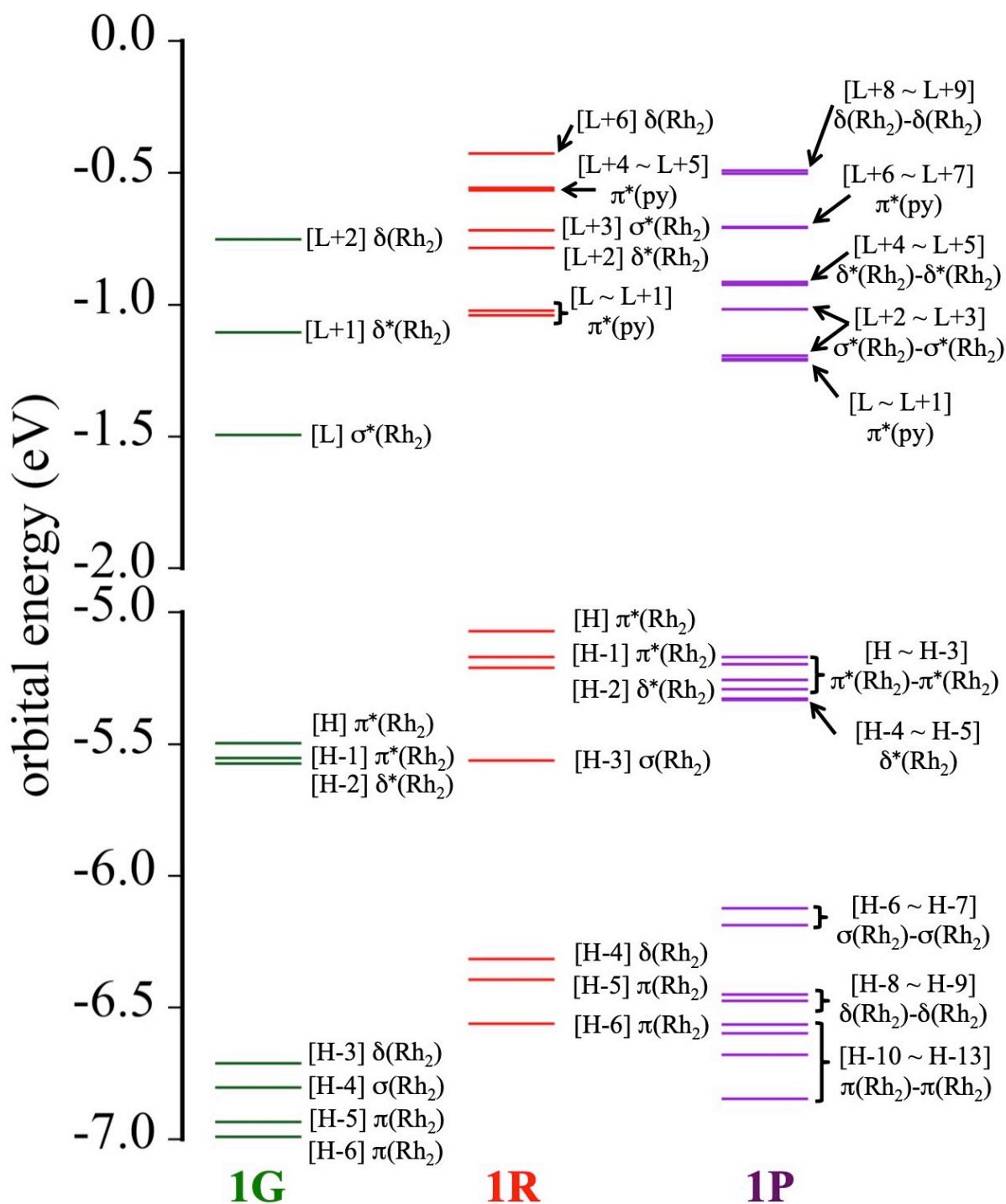


Fig. S14 MO configurations of **1G**, **1R**, and **1P**. Here, H and L are HOMO (highest occupied MO) and LUMO (lowest unoccupied MO), respectively.

Table S1. TDDFT results (absorption wavelength, oscillator strength, and dominant excitation character) of **1G**. Here, H and L are HOMO (highest occupied MO) and LUMO (lowest unoccupied MO), respectively.

Excitation	Wavelength (nm)	Oscillator strength (<i>f</i>)	Dominant excitation characters
S ₁	595.7	0.0030	H[$\pi^*(\text{Rh}_2)$] \rightarrow L[$\sigma^*(\text{Rh}_2)$] (88%)
S ₂	584.6	0.0024	H-1[$\pi^*(\text{Rh}_2)$] \rightarrow L[$\sigma^*(\text{Rh}_2)$] (86%) H[$\pi^*(\text{Rh}_2)$] \rightarrow L+1[$\delta^*(\text{Rh}_2)$] (10%)
S ₆	442.0	0.0012	H[$\pi^*(\text{Rh}_2)$] \rightarrow L+1[$\delta^*(\text{Rh}_2)$] (85%) H-1[$\pi^*(\text{Rh}_2)$] \rightarrow L[$\sigma^*(\text{Rh}_2)$] (10%)
S ₇	435.4	0.0016	H-1[$\pi^*(\text{Rh}_2)$] \rightarrow L+1[$\delta^*(\text{Rh}_2)$] (87%)

Table S2. TDDFT results (absorption wavelength, oscillator strength, and dominant excitation character) of **1R**. Here, H and L are HOMO (highest occupied MO) and LUMO (lowest unoccupied MO), respectively.

Excitation	Wavelength (nm)	Oscillator strength (<i>f</i>)	Dominant excitation characters
S ₂	520.7	0.0030	H[$\pi^*(\text{Rh}_2)$] \rightarrow L+3[$\sigma^*(\text{Rh}_2)$] (69%) H[$\pi^*(\text{Rh}_2)$] \rightarrow L+2[$\delta^*(\text{Rh}_2)$] (26%)
S ₃	511.4	0.0024	H-1[$\pi^*(\text{Rh}_2)$] \rightarrow L+3[$\sigma^*(\text{Rh}_2)$] (52%) H-1[$\pi^*(\text{Rh}_2)$] \rightarrow L+2[$\delta^*(\text{Rh}_2)$] (43%)
S ₅	444.2	0.0008	H[$\pi^*(\text{Rh}_2)$] \rightarrow L+2[$\delta^*(\text{Rh}_2)$] (68%) H[$\pi^*(\text{Rh}_2)$] \rightarrow L+3[$\sigma^*(\text{Rh}_2)$] (29%)
S ₆	430.9	0.0006	H-1[$\pi^*(\text{Rh}_2)$] \rightarrow L+2[$\delta^*(\text{Rh}_2)$] (51%) H-1[$\pi^*(\text{Rh}_2)$] \rightarrow L+3[$\sigma^*(\text{Rh}_2)$] (46%)

Table S3. TDDFT results (absorption wavelength, oscillator strength, and dominant excitation character) of **1P**. Here, H and L are HOMO (highest occupied MO) and LUMO (lowest unoccupied MO), respectively.

Excitation	Wavelength (nm)	Oscillator strength (<i>f</i>)	Dominant excitation characters
S ₁	560.5	0.0013	H[$\pi^*(\text{Rh}_2)$ - $\pi^*(\text{Rh}_2)$] \rightarrow L+3[$\sigma^*(\text{Rh}_2)$ - $\sigma^*(\text{Rh}_2)$] (29%) H-1[$\pi^*(\text{Rh}_2)$ - $\pi^*(\text{Rh}_2)$] \rightarrow L+2[$\sigma^*(\text{Rh}_2)$ - $\sigma^*(\text{Rh}_2)$] (13%) H[$\pi^*(\text{Rh}_2)$ - $\pi^*(\text{Rh}_2)$] \rightarrow L+2[$\sigma^*(\text{Rh}_2)$ - $\sigma^*(\text{Rh}_2)$] (11%) H-1[$\pi^*(\text{Rh}_2)$ - $\pi^*(\text{Rh}_2)$] \rightarrow L+3[$\sigma^*(\text{Rh}_2)$ - $\sigma^*(\text{Rh}_2)$] (10%)
S ₂	560.0	0.0029	H-1[$\pi^*(\text{Rh}_2)$ - $\pi^*(\text{Rh}_2)$] \rightarrow L+3[$\sigma^*(\text{Rh}_2)$ - $\sigma^*(\text{Rh}_2)$] (29%) H[$\pi^*(\text{Rh}_2)$ - $\pi^*(\text{Rh}_2)$] \rightarrow L+2[$\sigma^*(\text{Rh}_2)$ - $\sigma^*(\text{Rh}_2)$] (16%) H[$\pi^*(\text{Rh}_2)$ - $\pi^*(\text{Rh}_2)$] \rightarrow L+3[$\sigma^*(\text{Rh}_2)$ - $\sigma^*(\text{Rh}_2)$] (13%) H-1[$\pi^*(\text{Rh}_2)$ - $\pi^*(\text{Rh}_2)$] \rightarrow L+2[$\sigma^*(\text{Rh}_2)$ - $\sigma^*(\text{Rh}_2)$] (11%)
S ₄	555.9	0.0060	H-3[$\pi^*(\text{Rh}_2)$ - $\pi^*(\text{Rh}_2)$] \rightarrow L+2[$\sigma^*(\text{Rh}_2)$ - $\sigma^*(\text{Rh}_2)$] (41%) H-2[$\pi^*(\text{Rh}_2)$ - $\pi^*(\text{Rh}_2)$] \rightarrow L+3[$\sigma^*(\text{Rh}_2)$ - $\sigma^*(\text{Rh}_2)$] (22%) H-2[$\pi^*(\text{Rh}_2)$ - $\pi^*(\text{Rh}_2)$] \rightarrow L+4[$\delta^*(\text{Rh}_2)$ - $\delta^*(\text{Rh}_2)$] (15%)
S ₉	457.5	0.0024	H-1[$\pi^*(\text{Rh}_2)$ - $\pi^*(\text{Rh}_2)$] \rightarrow L+4[$\delta^*(\text{Rh}_2)$ - $\delta^*(\text{Rh}_2)$] (29%) H[$\pi^*(\text{Rh}_2)$ - $\pi^*(\text{Rh}_2)$] \rightarrow L+5[$\delta^*(\text{Rh}_2)$ - $\delta^*(\text{Rh}_2)$] (25%) H[$\pi^*(\text{Rh}_2)$ - $\pi^*(\text{Rh}_2)$] \rightarrow L+2[$\sigma^*(\text{Rh}_2)$ - $\sigma^*(\text{Rh}_2)$] (22%)
S ₁₃	437.4	0.0013	H-3[$\pi^*(\text{Rh}_2)$ - $\pi^*(\text{Rh}_2)$] \rightarrow L+5[$\delta^*(\text{Rh}_2)$ - $\delta^*(\text{Rh}_2)$] (29%) H-2[$\pi^*(\text{Rh}_2)$ - $\pi^*(\text{Rh}_2)$] \rightarrow L+4[$\delta^*(\text{Rh}_2)$ - $\delta^*(\text{Rh}_2)$] (25%) H-2[$\pi^*(\text{Rh}_2)$ - $\pi^*(\text{Rh}_2)$] \rightarrow L+3[$\sigma^*(\text{Rh}_2)$ - $\sigma^*(\text{Rh}_2)$] (24%)
S ₁₈	415.0	0.0006	H-2[$\pi^*(\text{Rh}_2)$ - $\pi^*(\text{Rh}_2)$] \rightarrow L+8[$\delta(\text{Rh}_2)$ - $\delta(\text{Rh}_2)$] (36%) H-3[$\pi^*(\text{Rh}_2)$ - $\pi^*(\text{Rh}_2)$] \rightarrow L+9[$\delta(\text{Rh}_2)$ - $\delta(\text{Rh}_2)$] (28%) H-3[$\pi^*(\text{Rh}_2)$ - $\pi^*(\text{Rh}_2)$] \rightarrow L+8[$\delta(\text{Rh}_2)$ - $\delta(\text{Rh}_2)$] (10%)

References

- S1. Y. Kataoka, N. Yano, T. Kawamoto, M. Handa, *Eur. J. Inorg. Chem.* 2015, 34, 5650.
- S2. M. C. Burla, R. Caliendo, M. Camalli, B. Carrozzini, G. L. Casciaro, L. De Caro, C. Giacovazzo, G. Polidori, R. Spagna, *J. Appl. Cryst.*, 2005, **38**, 381.
- S3. M. C. Burla, R. Caliendo, M. Camalli, B. Carrozzini, G. L. Casciaro, C. Giacovazzo, M. Mallamo, A. Mazzone, G. Polidori, R. Spagna, *J. Appl. Cryst.*, 2012, **45**, 351.
- S4. G. M. Sheldrick, *Acta Cryst.*, 2015, **A71**, 3.
- S5. G. M. Sheldrick, *Acta Cryst.*, 2015, **C71**, 3.
- S6. Gaussian 09, Revision C.02, M. J. Frisch, G. W. Trucks, H. B. Schlegel, G. E. Scuseria, M. A. Robb, J. R. Cheeseman, G. Scalmani, V. Barone, G. A. Petersson, H. Nakatsuji, X. Li, M. Caricato, A. Marenich, J. Bloino, B. G. Janesko, R. Gomperts, B. Mennucci, H. P. Hratchian, J. V. Ortiz, A. F. Izmaylov, J. L. Sonnenberg, D. Williams-Young, F. Ding, F. Lipparini, F. Egidi, J. Goings, B. Peng, A. Petrone, T. Henderson, D. Ranasinghe, V. G. Zakrzewski, J. Gao, N. Rega, G. Zheng, W. Liang, M. Hada, M. Ehara, K. Toyota, R. Fukuda, J. Hasegawa, M. Ishida, T. Nakajima, Y. Honda, O. Kitao, H. Nakai, T. Vreven, K. Throssell, J. A. Montgomery, Jr., J. E. Peralta, F. Ogliaro, M. Bearpark, J. J. Heyd, E. Brothers, K. N. Kudin, V. N. Staroverov, T. Keith, R. Kobayashi, J. Normand, K. Raghavachari, A. Rendell, J. C. Burant, S. S. Iyengar, J. Tomasi, M. Cossi, J. M. Millam, M. Klene, C. Adamo, R. Cammi, J. W. Ochterski, R. L. Martin, K. Morokuma, O. Farkas, J. B. Foresman, and D. J. Fox, Gaussian, Inc., Wallingford CT, 2016.